Silicon-on-insulator polarization splitting and rotating device for polarization diversity circuits

Liu, Liu; Ding, Yunhong; Yvind, Kresten; Hvam, Jørn Märcher

Published in:
Optics Express

Link to article, DOI:
10.1364/OE.19.012646

Publication date:
2011

Document Version
Publisher's PDF, also known as Version of record

Silicon-on-insulator polarization splitting and rotating device for polarization diversity circuits

Liu Liu,[1,2,*] Yunhong Ding,[2,3] Kresten Yvind,[2] and Jørn M. Hvam[2]

[1]*School for Information and Optoelectronic Science and Engineering, South China Normal University, 510006 Guangzhou, China*
[2]*DTU-Fotonik, Technical University of Denmark, Ørsteds Plads Building 343, 2800 Lyngby, Denmark*
[3]*Wuhan National Laboratory for Optoelectronics, School of Optoelectronics Science and Engineering, Huazhong University of Science and Technology, 430074 Wuhan, China*
**realdream.liuliu@gmail.com*

Abstract: A compact and efficient polarization splitting and rotating device built on the silicon-on-insulator platform is introduced, which can be readily used for the interface section of a polarization diversity circuit. The device is compact, with a total length of a few tens of microns. It is also simple, consisting of only two parallel silicon-on-insulator wire waveguides with different widths, and thus requiring no additional and nonstandard fabrication steps. A total insertion loss of −0.6dB and an extinction ratio of 12dB have been obtained experimentally in the whole C-band.

OCIS codes: (130.3120) Integrated optics devices; (130.5440) Polarization-selective devices.

References and links

1. W. Bogaerts, R. Baets, P. Dumon, V. Wiaux, S. Beckx, D. Taillaert, B. Luyssaert, J. Van Campenhout, P. Bienstman, and D. Van Thourhout, "Nanophotonic waveguides in silicon-on-insulator fabricated with CMOS technology," J. Lightwave Technol. **23**(1), 401–412 (2005).
2. T. Tsuchizawa, K. Yamada, H. Fukuda, T. Watanabe, J. Takahashi, M. Takahashi, T. Shoji, E. Tamechika, S. Itabashi, and H. Morita, "Microphotonics devices based on silicon microfabrication technology," IEEE J. Sel. Top. Quantum Electron. **11**(1), 232–240 (2005).
3. C. Manolatou, S. G. Johnson, S. Fan, P. R. Villeneuve, H. A. Haus, and J. D. Joannopoulos, "High density integrated optics," J. Lightwave Technol. **17**(9), 1682–1692 (1999).
4. T. Barwicz, M. R. Watts, M. A. Popović, P. T. Rakich, L. Socci, F. X. Kärtner, E. P. Ippen, and H. I. Smith, "Polarization-transparent microphotonic devices in the strong confinement limit," Nat. Photonics **1**(1), 57–60 (2007).
5. W. Bogaerts, D. Taillaert, P. Dumon, D. Van Thourhout, R. Baets, and E. Pluk, "A polarization-diversity wavelength duplexer circuit in silicon-on-insulator photonic wires," Opt. Express **15**(4), 1567–1578 (2007), http://www.opticsinfobase.org/abstract.cfm?URI=oe-15-4-1567.
6. H. Fukuda, K. Yamada, T. Tsuchizawa, T. Watanabe, H. Shinojima, and S. Itabashi, "Silicon photonic circuit with polarization diversity," Opt. Express **16**(7), 4872–4880 (2008), http://www.opticsinfobase.org/abstract.cfm?URI=oe-16-7-4872.
7. H. Fukuda, K. Yamada, T. Tsuchizawa, T. Watanabe, H. Shinojima, and S. Itabashi, "Ultrasmall polarization splitter based on silicon wire waveguides," Opt. Express **14**(25), 12401–12408 (2006), http://www.opticsinfobase.org/oe/abstract.cfm?uri=oe-14-25-12401.
8. L. Liu, Y. Ding, K. Yvind, and J. M. Hvam, "Efficient and compact TE-TM polarization converter built on silicon-on-insulator platform with a simple fabrication process," Opt. Lett. **36**(7), 1059–1061 (2011).
9. H. Deng, D. O. Yevick, C. Brooks, and P. E. Jessop, "Design rules for slanted-angle polarization rotators," J. Lightwave Technol. **23**(1), 432–445 (2005).
10. M. R. Watts, and H. A. Haus, "Integrated mode-evolution-based polarization rotators," Opt. Lett. **30**(2), 138–140 (2005).
11. H. Fukuda, K. Yamada, T. Tsuchizawa, T. Watanabe, H. Shinojima, and S. Itabashi, "Polarization rotator based on silicon wire waveguides," Opt. Express **16**(4), 2628–2635 (2008), http://www.opticsinfobase.org/abstract.cfm?URI=oe-16-4-2628.
12. Y. Yue, L. Zhang, M. Song, R. G. Beausoleil, and A. E. Willner, "Higher-order-mode assisted silicon-on-insulator 90 degree polarization rotator," Opt. Express **17**(23), 20694–20699 (2009), http://www.opticsinfobase.org/abstract.cfm?URI=oe-17-23-20694.
13. Z. Wang, and D. Dai, "Ultrasmall Si-nanowire-based polarization rotator," J. Opt. Soc. Am. B **25**(5), 747–753 (2008).
14. K. Bayat, S. K. Chaudhuri, and S. Safavi-Naeini, "Ultra-compact photonic crystal based polarization rotator," Opt. Express **17**(9), 7145–7158 (2009), http://www.opticsinfobase.org/abstract.cfm?uri=oe-17-9-7145.

#145637 - $15.00 USD Received 11 Apr 2011; revised 18 May 2011; accepted 30 May 2011; published 15 Jun 2011

15. J. Zhang, M. Yu, G. Lo, and D. L. Kwong, "Silicon waveguide based mode-evolution polarization rotator," IEEE J. Sel. Top. Quantum Electron. **16**(1), 53–60 (2010).
16. FIMMWAVE/FIMMPROP, Photon Design Ltd, http://www.photond.com.

1. Introduction

Silicon-on-insulator (SOI) has been considered recently as a promising platform for photonic circuits, largely driven by the CMOS-compatible fabrication technology and the high refractive-index contrast of the waveguide structure [1,2]. High-density integration and mass production of devices are therefore made possible. On the other hand, this high index contrast also induces a large polarization dependent dispersion or loss for normal components [3], and makes SOI inconvenient to integrate with other polarization insensitive platforms, like optical fiber networks. Instead of pursuing difficult polarization-independent devices on SOI, a polarization diversity scheme could be employed [4–6]. In this case, the orthogonal polarization components of the input light are first split into two different waveguides by using a polarization splitter [7]. A polarization rotator is then employed in one of the waveguides to rotate the polarization 90° [8–15]. Therefore, for the rest of the photonic chip only one polarization has to be processed. At the output, a copy of the polarization rotator and splitter can be implemented in order to combine the two polarizations without interference. We have successfully demonstrated a compact and efficient polarization converter on SOI based on the cross-polarization coupling between two SOI wires waveguide with different widths [8]. As compared to other polarization converters [9–15], this structure can be fabricated together with common deeply-etched SOI wire waveguides and devices, and thus requires no additional fabrication steps.

In this paper, we further extend the ability of the polarization converter in [8], and show that such a single device structure can be used for polarization splitting and rotating (PSR) simultaneously. Thus, a polarization diversity scheme on SOI can be readily implemented. We theoretically study the transmission properties of the proposed device. The optimized structures are also fabricated and characterized experimentally.

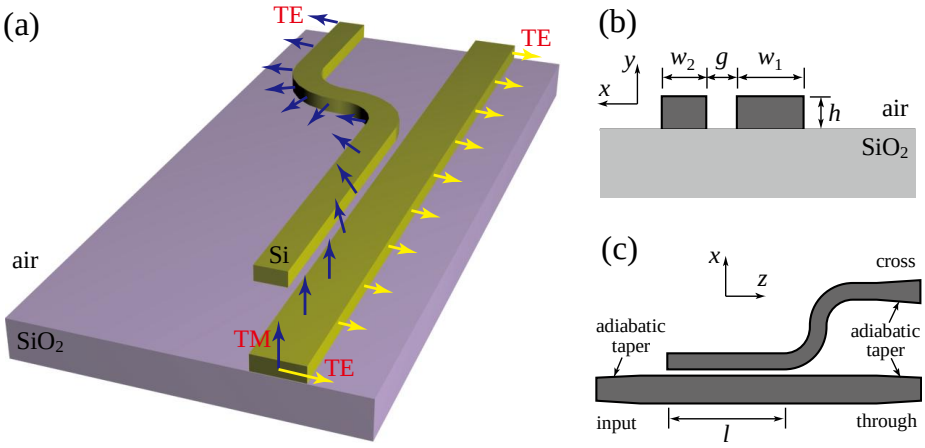

Fig. 1. Schematic structure and working principle of the proposed polarization splitter and rotator. (a) three-dimensional model; (b) *x*-*y* cross-section; (c) *x*-*z* cross-section.

2. Design and simulation

The structure of the present PSR device is sketched in Fig. 1. It consists of two parallel SOI photonic wire waveguides coupled to each other. In order to achieve an efficient cross-polarization coupling, air is employed as the top-cladding. The widths (w_1 and w_2) of the two waveguides (waveguide 1 and waveguide 2, respectively) are adjusted so that the effective index of the fundamental transverse-magnetic (TM) mode in waveguide 1 is equal to that of

#145637 - $15.00 USD Received 11 Apr 2011; revised 18 May 2011; accepted 30 May 2011; published 15 Jun 2011

the fundamental transverse-electric (TE) mode in waveguide 2, i.e., $n_{eff}^{1,TM} = n_{eff}^{2,TE}$, which is usually called the phase matching condition. In this case, an efficient coupling between these two modes can be achieved [8]. The effective index of a single SOI wire waveguide with air top-cladding at different widths is shown in Fig. 2. Here, we choose w_1 = 600 nm and w_2 = 333 nm. The height h of the silicon waveguide layer is 250 nm, which is also the parameter of the SOI wafer used in the experiments. On the other hand, at the chosen widths the effective index $n_{eff}^{1,TE}$ of the TE mode in waveguide 1 is very different from that of any guided mode in waveguide 2 (cf. Figure 2). Therefore, according to the coupling mode theory the TE mode in waveguide 1 is expected to pass freely across the device. In general, such a structure in Fig. 1 exhibits the abilities to couple the TM mode from the input waveguide to the adjacent waveguide and simultaneously convert it into a TE mode, while leave the TE mode untouched in the input waveguide. This is exactly the characteristic of the interface section of a polarization diversity circuit, which is conventionally constructed by cascading an individual polarization splitter and rotator [4–6]. A similar structure of two SOI waveguides with the same width was used as a polarization splitter [7]. In the proposed structure, an additional functionality of polarization rotation can be achieved.

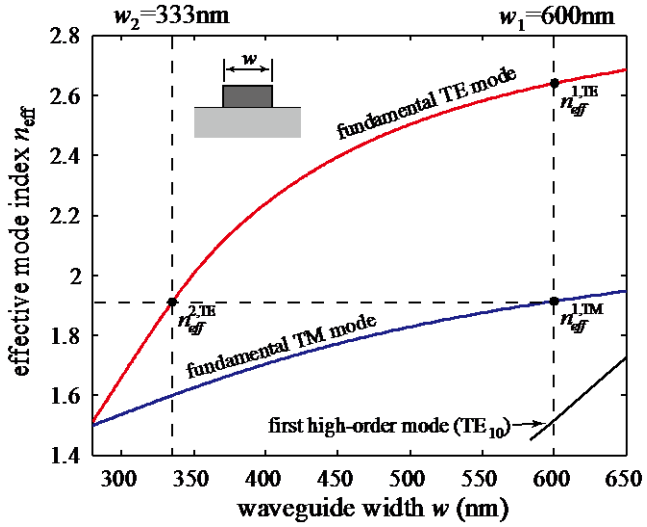

Fig. 2. Effective indices of the fundamental TE and TM modes of an air-cladded SOI wire waveguide with different widths w. The model is shown in the inset. h = 250 nm.

The propagation of the optical field in the proposed device is first studied by a three-dimensional finite-difference time-domain (3D-FDTD) method, as shown in Fig. 3. The gap g here is 100 nm, and the rest of the structural parameters are the same as above. One can clearly see that the input TM mode in waveguide 1 is gradually converted to the TE mode in waveguide 2 along the propagation direction. There exists an optimal coupling length for the maximal conversion, beyond which the optical power is coupled back to waveguide 1. As for the input TE mode, the optical power is all confined in waveguide 1 across the whole device. These results comply with the discussions in the previous paragraph. It is worthwhile to note that the discretization lattice here is set to a rather large value, i.e. 20 nm, which is not fine enough to describe the dimensions of the structure accurately. Further refining the grid will, however, make the simulation effort unaffordable with the calculation resources at hand. Thus, the results shown in Fig. 3 are just qualitative analyses.

#145637 - $15.00 USD Received 11 Apr 2011; revised 18 May 2011; accepted 30 May 2011; published 15 Jun 2011

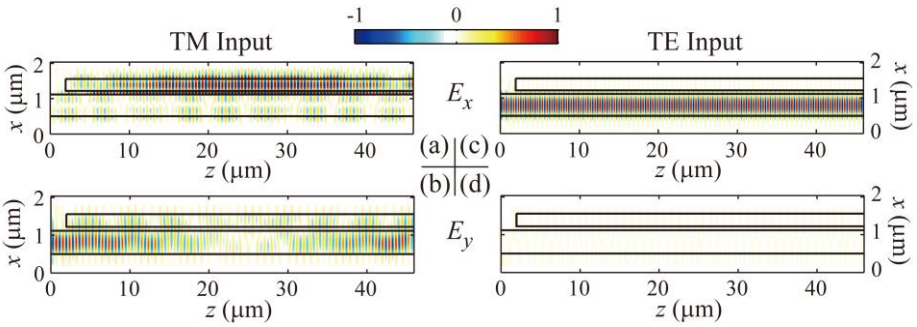

Fig. 3. Time snap-shots of the fields at steady state within the *x*-*z* plane which lies at the center of the SOI wire waveguide in the *y* direction. The simulation is done by 3D-FDTD with w_1 = 600 nm, w_2 = 333 nm, g = 100 nm, and h = 250 nm. The wavelength is 1550 nm. (a) and (b) are for the case of the TM mode input; (c) and (d) are for the case of the TE mode input. (a) and (c) are distributions of the E_x fileld; (b) and (d) are distributions of the E_y fileld.

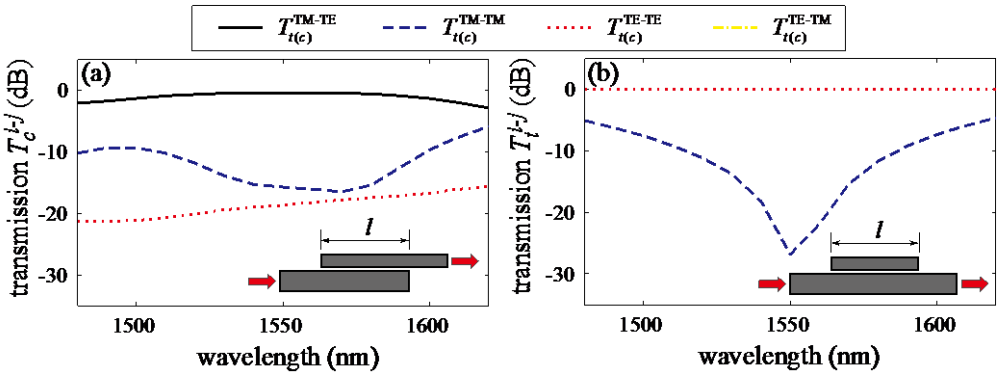

Fig. 4. Simulated transmission coefficients between differently polarized modes from the input-port to the cross-port (a) and the through-port (b). The models are shown in the insets respectively. Here, w_1 = 600 nm, w_2 = 333 nm, g = 100 nm, h = 250 nm, and l = 36.8 μm. The transmission coefficients which are not presented are well below –35dB.

In order to model accurately the transmission properties of the proposed device, a mode expansion and matching method [16] is then employed, which is more suitable to deal with the structure involved here. Figure 4 shows the transmission coefficients $T_{t(c)}^{i-j}$ when the coupling length l = 36.8 μm. Here, the subscript t or c indicates the response at the through-port or cross-port of the device (cf., Fig. 1), respectively. The superscript *i*-*j*, where *i*, *j* can be TE or TM, means the transmission from mode *i* at the input to mode *j* at the output. Considering the complexity, the simulation model is reduced correspondingly as shown in the insets of Fig. 4, where the bending sections are neglected. For the through-port response shown in Fig. 4(b), T_t^{TE-TE} remains close to 1 in the whole wavelength range of simulation. On the other hand, the TM mode from the input port is suppressed at the through port, and a dip is observed in the T_t^{TM-TM} curve at 1550 nm wavelength, which corresponds to the position where the phase-matching condition is fulfilled between the fundamental TM mode in waveguide 1 and the fundamental TE mode in waveguide 2. Accordingly, a peak is observed in the T_c^{TM-TE} curve shown in Fig. 4(a), which reaches 90%, corresponding to an overall insertion loss of –0.46dB. The unconverted TM mode power remains partly in the through-port (T_t^{TM-TM}) and the cross-port (T_c^{TM-TM}). They become the main source of cross-talk for the proposed device. Nevertheless, the extinction ratio is still better than 13dB in the whole C-band (1530 nm—1565 nm).

#145637 - $15.00 USD Received 11 Apr 2011; revised 18 May 2011; accepted 30 May 2011; published 15 Jun 2011

Similar to a common directional coupler on the SOI platform, the proposed PSR device also has a tight tolerance to the variations in device dimensions, e.g., waveguide widths. A slight deviation from the designed value will make the phase-matching condition fail, which will mainly result in a decrease in the efficiency of the cross-polarization coupling at the desired wavelength. We further study the influence of the variation in w_1 on the device performance. Figure 5(a) shows the cross-port responses with w_1 = 332 nm, 333 nm, and 334 nm. One finds that the coupling wavelength peaking $T_c^{\text{TM-TE}}$ shifts with a rate of about 15 nm/nm with respect to the variation of w_1. Figure 5(b) shows the relation between w_1 and w_2 in order to maintain the phase-matching condition at 1550 nm. It is almost a linear curve with a slop of about 12, which implies that the device performance is much less sensitive to the variation of w_2. This sensitivity difference can be explained by the local derivatives of the two curves shown in Fig. 2 at the working point. We also find that employing larger waveguide widths will improve the extinction ratio at the output and decrease the sensitivity to the dimension variations. On the other hand, this will weaken the strength of the cross-polarization coupling and increase the device length. A large waveguide cross-section will also make the effective indices of the high-order modes more close to those of the working fundamental modes (cf., Fig. 2). This will introduce unwanted coupling to those modes.

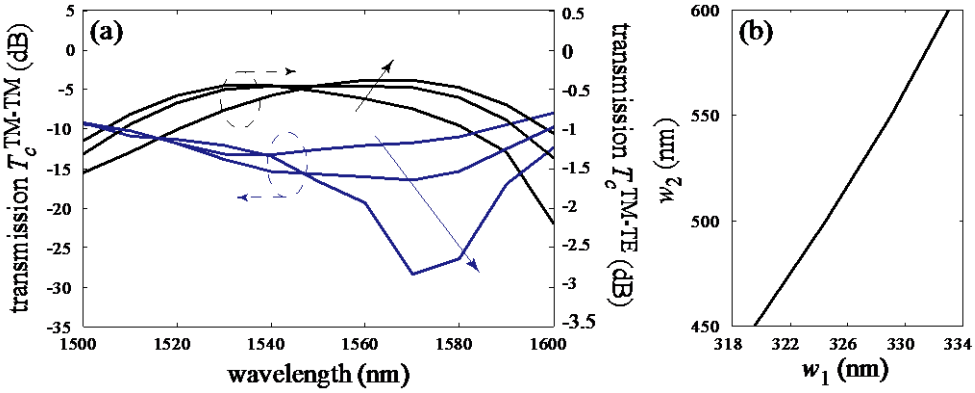

Fig. 5. (a) Simulated transmission coefficients. Here, w_2 = 332 nm, 333 nm, 334 nm along the solid arrow direction, and the rest of the parameters are the same as those in Fig. 4. (b) Relation between w_1 and w_2 in order to maintain the phase-matching condition at 1550 nm.

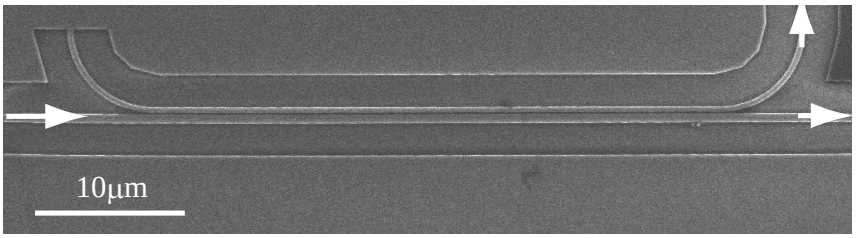

Fig. 6. Scanning electron microscope picture of a fabricated device. Arrows indicate propagation directions of the light.

3. Experiment and measurement

We fabricated the designed devices on a commercial SOI wafer using E-beam lithography (JEOL JBX-9300FS) and dry etching technologies. A picture of a finished device is shown in Fig. 6. Adiabatic tapers were used at the input and two output ports for connecting with the standard single-mode SOI waveguide of 450 nm wide in the rest of the circuit [cf., Fig. 1(c)]. The fabricated samples were cleaved for characterization. The waveguides were tapered up to a width of 4 μm at the cleaved facets for better coupling with lensed fibers. The measurement

#145637 - $15.00 USD Received 11 Apr 2011; revised 18 May 2011; accepted 30 May 2011; published 15 Jun 2011

results are illustrated in Fig. 7. We refer to Ref [8]. for the detailed measurement setup and calibration procedure. In general, the measured transmission curves are matching well those from the simulations in Fig. 4. The overall insertion loss and extinction ratio in the whole C-band is about −0.6dB and 12dB, respectively, slightly worse than the simulation results. Judged by the period, the fast oscillations observed in, e.g., the $T_c^{\text{TM-TM}}$ curve is likely due to a slight error in calibrating the measurement setup [7,8]. The fabrication repeatability of the proposed device was also studied. Figure 8 shows the measured $T_c^{\text{TM-TE}}$ curves for two PSR devices with the same designed parameters and on the same die. A good consistency can be found. Further investigation on improving the cross-die stability is also undertaken.

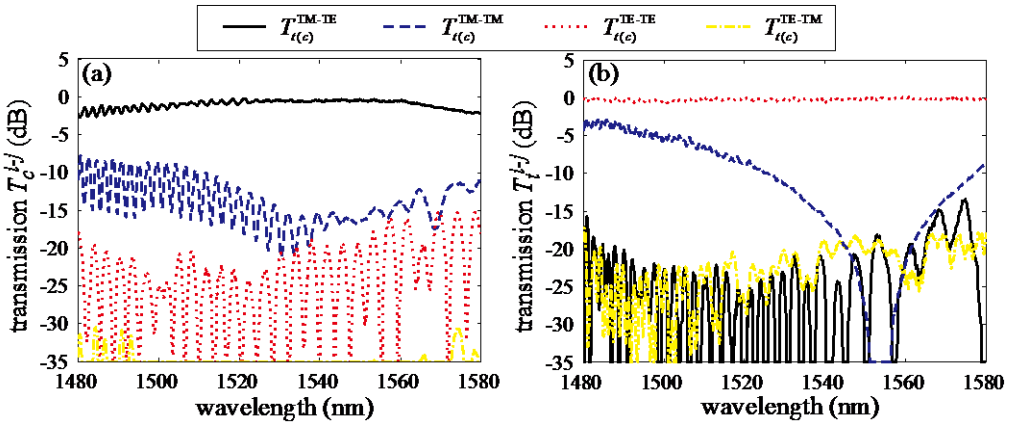

Fig. 7. Measured transmission coefficients between different polarized modes from the input-port to the cross-port (a) and the through-port (b).

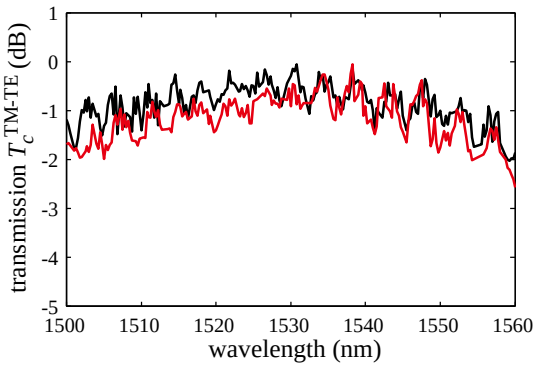

Fig. 8. Measured transmission coefficient $T_c^{\text{TM-TE}}$ of two PSR devices with the same parameters on one SOI die.

4. Conclusion

We have introduced a compact SOI-based PSR device used for the interface section of a polarization diversity circuit. The device is based on the cross-polarization coupling effect between two parallel SOI wire waveguides with air top-cladding, which can be fabricated in one lithography and etching step as needed for making the rest of the SOI circuit. We have demonstrated that such a single device structure can act as an efficient polarization splitter and rotator simultaneously. A total insertion loss of −0.6dB and an extinction ratio of 12dB have been obtained experimentally for a fabricated device.

#145637 - $15.00 USD Received 11 Apr 2011; revised 18 May 2011; accepted 30 May 2011; published 15 Jun 2011